A Reference Modification Model Digitally Controlled DC–DC Converter for Improvement of Transient Response

Fujio Kurokawa, *Fellow, IEEE*, Akihiro Yamanishi, and Shota Hirotaki, *Student Member, IEEE*

***Abstract*—This paper presents a reference modification model digitally controlled dc–dc converter. The proposed method is able to obtain superior transient response because it modifies a reference of conventional feedback loop against the change of output voltage. The modifying process operates only in the transient state. During the steady state, the feedforward control cancels a steady-state-error. Since the feedforward control uses the load current value, this paper discusses two current-sensing methods. One is the output current-sensing method using the sensing resistor, and the reactor current-sensing method using the *R–C* filter is discussed in order to reduce a performance loss by the sensing resistor. As a result, the output current-sensing method is effective in case that high-transient-response performance is required. On the other hand, it is better to use the reactor current-sensing method when efficiency is important.**

***Index Terms*—Current-sensing, dc–dc power converters, digital control, performance loss, transient response.**

I. Introduction

THE importance of energy saving, including energy management, has been further increasing due to the ongoing global warming in the power supply system. The transient response is also important because a low-power sleep mode and a high-power active mode are changed alternately. The power supply system requires an excellent one against both the energy management function and the transient response. A digital control technology has an intelligent function that an analog control technology does not have. The digital control technology of switching power supply has made remarkable progress in order to satisfy these requirements [1]–[7]. However, it is important to improve transient characteristics because both the conversion time of A–D converter and the processing time of digital controller exert a bad influence on it [8]–[14]. We accept the delay time and have focused to solve its problem by the intelligent arithmetic algorithm. The steady-state characteristics are also important in the power supply system.

We have already reported a static model dc–dc converter using voltage controlled oscillator (VCO) [15]–[18]. This method has no steady-state characteristics because calculation equations of the static model are applied to the reference in P control of the conventional feedback loop. As a result, it is possible to regulate the output voltage without depending on the integral control. On the other hand, the control by conventional feedback loop is mainly against transient characteristics because the input–output characteristic in the steady-state derives equations of a simple static model; it has a limit to improve transient characteristics. Furthermore, since the reference of output voltage is modified with the VCO, the integration of both the VCO and the digital logic circuit is difficult and impractical. Then, we have also reported a steady-state-error and transient suppression (STS) model dc–dc converter using a general A–D converter [19]–[21]. In [19]–[21], no steady-state characteristics can be obtained against the change of input voltage and output current by the existing static model to the bias of the conventional feedback loop. Although transient characteristics are also suppressed sufficiently by adding the exponential function to calculation equations of the existing static model, the effectiveness against transient suppression is limited to a specific load for the step change. There is no control parameter that is able to adapt against various variation width of the load for the step change. Therefore, it is necessary to add a new technique to control unit, including static model, in order to suppress the transient characteristics against various widths of the load for the step change.

The purpose of this paper is to present the digitally controlled dc–dc converter using a reference modification model for improvement of the transient response. In the previously presented model control [22], only bias value of PID control is modified to compensate the feed forward control pass in both steady and transient states. Reference is operated to suppress the over/undershoot of output voltage only in the transient state. On the other hand, not only the bias but also the reference of PID control is modified in this paper. The name of presented model is called the reference modification model. The digital circuit configuration and algorithm of proposed model are simple compared with other model methods [23]–[25], and superior dynamic characteristics are obtained. Although the existing static model senses the load current value, this paper discusses two current-sensing methods. One is the output current-sensing method using the sensing resistor, the other is the reactor current-sensing method using the *R–C* filter [22], [26]. The second method is able to reduce the performance loss of the sensing resistor. At first, the configurations of proposed digitally controlled dc–dc converter and its operation principle are described. Next, the design criteria of control parameters are shown, and performance characteristics are evaluated in both methods.

Manuscript received September 16, 2014; revised December 31, 2014; accepted March 1, 2015. Date of publication March 19, 2015; date of current version September 21, 2015. Recommended for publication by Associate Editor M. Ferdowsi.

The authors are with the Nagasaki University, Nagasaki 852-8521, Japan (e-mail: fkurokaw@nagasaki-u.ac.jp; yappari_kahlua_milk@yahoo.co.jp; e0h2031@gmail.com).

Digital Object Identifier 10.1109/TPEL.2015.2411679

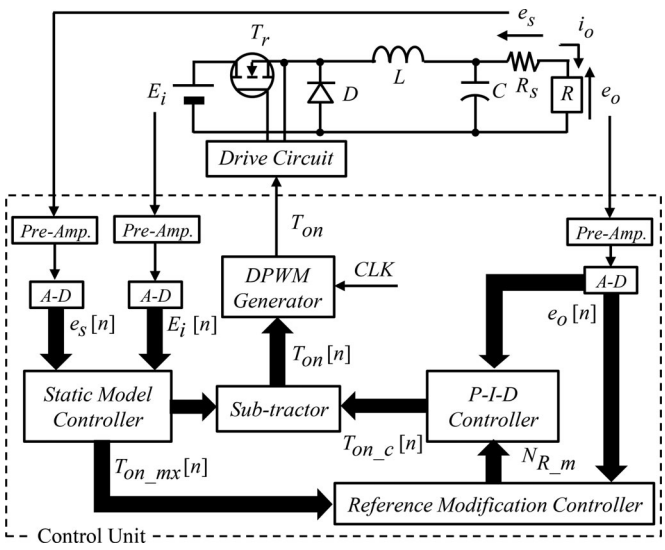

Fig. 1. Proposed digital controlled dc–dc converter by output current-sensing method.

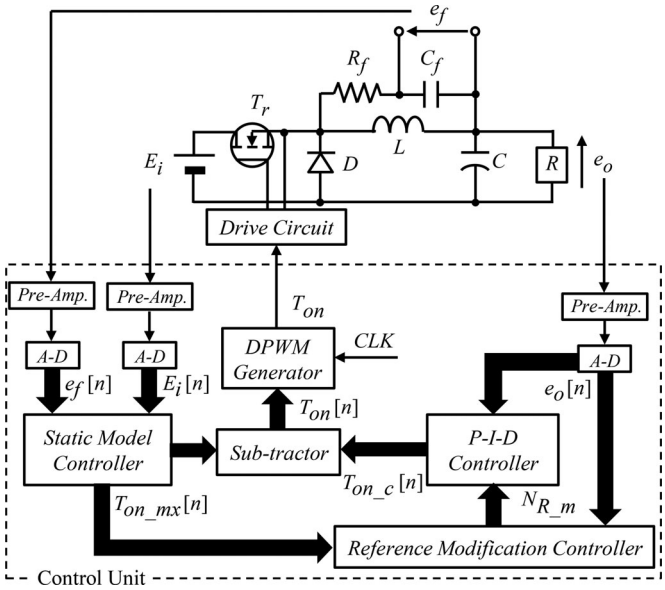

Fig. 2. Proposed digital controlled dc–dc converter by reactor current-sensing method.

As a result, the output current-sensing method is effective in case that high-transient-response performance is required. On the other hand, it is better to use the reactor current-sensing method when efficiency is important. Therefore, the proposed method using the output current-sensing method is useful to realize the high-performance digital control circuit for dc–dc converter because it can satisfy requirements against both steady and transient states.

II. Operation Principle

Figs. 1 and 2 show the proposed digital controlled dc–dc converter using the output current-sensing method and the reactor

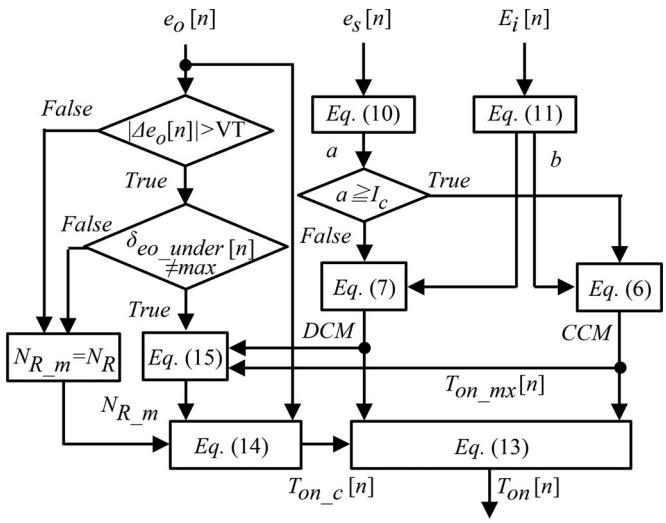

Fig. 3. Flowchart of proposed method by output current sensing.

current-sensing method. In Figs. 1 and 2, E_i is the input voltage, e_o is the output voltage, R is the load resistance, L is the inductor, C is the smoothing capacitor, D is the diode, T_r is the switch, R_s and es are the sensing resistor to sense the output current i_o and its voltage, and R_f and C_f are, respectively, the filter's resistor and capacitor for the reactor current-sensing, respectively. In the control unit against the output current-sensing method, e_o is sensed as feedback and E_i and i_o are sensed as feed forward. On the other hand, in the reactor current-sensing method, the reactor current i_L is sensed instead of i_o. i_L is sensed by measuring the capacitor voltage e_f from the R–C filter in parallel with the power stage of inductor. Equation (1) shows the relational equation between e_f and i_L [22]

$$E_f(s) = I_L(s) \cdot r_L \cdot \frac{1 + s \cdot L/r_L}{1 + s \cdot R_f C_f} = I_L(s) \cdot r_L \cdot \frac{1 + s \cdot \tau_L}{1 + s \cdot \tau_f}. \tag{1}$$

In (1), τ_L and τ_f expresses L/r_L and $R_f C_f$, respectively. When parameters of the filter are selected as $\tau_L = \tau_f$, the filter's capacitor voltage is equal to the product of the inductor's internal resistance r_L and i_L.

The proposed control circuit consists of A–D converters, preamplifiers, the PID controller, the static model controller, the reference modification controller, and the subtractor. At first, the sensed voltages are converted to the digital value by A–D converters and preamplifiers. The following equations show the relational equation between the sensed voltage and its digital value:

$$e_o[n] = A_{eo} G_{eo} e_o = G_{Aeo} e_o \tag{2}$$

$$E_i[n] = A_{Ei} G_{Ei} E_i = G_{AEi} E_i \tag{3}$$

$$e_s[n] = A_{es} G_{es} R_s i_o = G_{Aes} R_s i_o \tag{4}$$

$$E_f[n] = A_{ef} G_{ef} r_L i_L = G_{Aef} r_L i_L. \tag{5}$$

In (2) through (5), $e_o[n]$ is the digital value for e_o and A_{e_o} and G_{e_o} are the circuit gains of the preamplifier and the A–D converter to sense e_o. $E_i[n]$ is the digital value for E_i and A_{E_i}

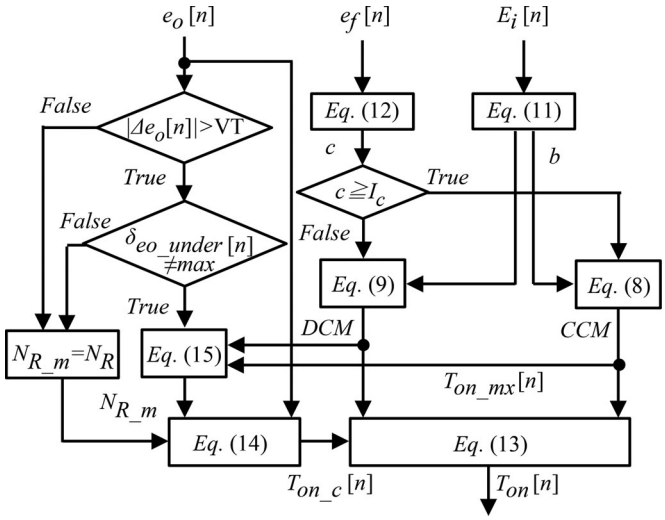

Fig. 4. Flowchart of proposed method by reactor current sensing.

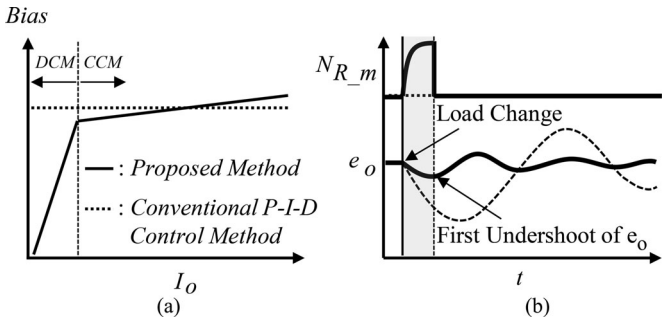

Fig. 5. Operation characteristics of proposed method. (a) Bias. (b) Reference value.

and G_{E_i} are the circuit gains of the preamplifier and the A–D converter to sense E_i. $e_s[n]$ is the digital value for *es*, A_{e_s} and G_{e_s} are the circuit gains of the preamplifier and the A–D converter to sense e_s. Similarly, $E_f[n]$ is the digital value for e_f and A_{e_f} and G_{e_f} are the circuit gains of the preamplifier and the A–D converter to sense e_f. Moreover, A_{e_o},G_{e_o}, $A_{E_i}G_{E_i}$, $A_{e_s}G_{e_s}$, and $A_{e_f}G_{e_f}$ are unified to $G_{A_{e_o}}$, $G_{A_{E_i}}$, $G_{A_{e_s}}$, and $G_{A_{e_f}}$, respectively.

In the static model controller, the calculation result by the existing static model is sent to the reference modification controller and the subtractor. The calculation equation of $T_{on\_mx}[n+1]$ is derived from the relational equation of the input–output characteristic in the steady state [27]. Equations (6)–(9) are the calculation equations of $T_{on\_mx}[n+1]$ against the output current-sensing method and the reactor current-sensing method. Equations (6) and (7) show equations against $T_{on\_mx}[n+1]$ of the output current-sensing method

$$T_{on\_mc}[n+1] = \frac{N_{Ts}\,(E_o^* + ra)}{b} + N_{Bc} \tag{6}$$

$$T_{on\_md}[n+1] = N_{Ts}\sqrt{\frac{2E_o^* La}{b\,(b-E_o^*)\,T_s}} + N_{Bd}. \tag{7}$$

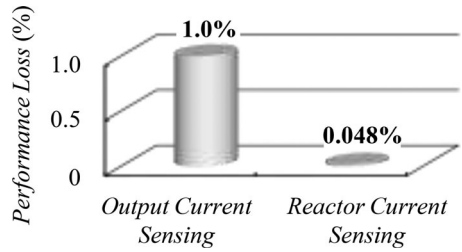

Fig. 6. Performance loss against each current sensing.

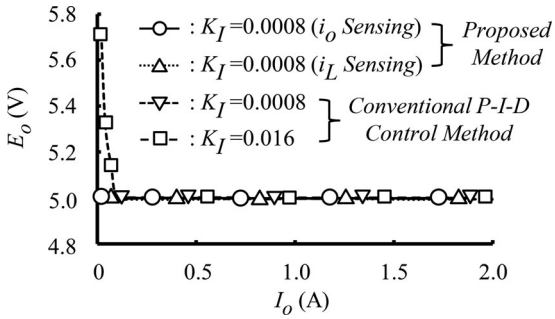

Fig. 7. Experimental regulation characteristics of each control method.

Equations (8) and (9) show equations against $T_{on\_mx}[n+1]$ of the reactor current-sensing method

$$T_{on\_mc}[n+1] = \frac{N_{Ts}\,(E_o^* + rc)}{b} + N_{Bc} \tag{8}$$

$$T_{on\_md}[n+1] = N_{Ts}\sqrt{\frac{2E_o^* Lc}{b\,(b-E_o^*)\,T_s}} + N_{Bd}. \tag{9}$$

Equations (6) and (8) are the equation $T_{on\_mc}[n+1]$ of continuous current mode (CCM), and (7) and (9) are the equation $T_{on\_md}[n+1]$ of discontinuous current mode (DCM). $T_{on\_mx}[n+1]$ is equal to $T_{on\_mc}[n+1]$ in case of CCM, while $T_{on\_mx}[n+1]$ is equal to $T_{on\_md}[n+1]$ in case of DCM. In (6) through (9), E_o^* is the desired output voltage, *Ts* and N_{T_s} are the switching period and its digital value, and *r* is the aggregate loss resistance in the circuit. N_{Bc} and N_{Bd} are the reference bias of each current region. The index *n* denotes the *n*th switching period. *a*, *b*, and *c* are the converted values to analog values; they are, respectively, i_o, E_i, and i_L and are given as follows:

$$a = \frac{e_s[n]}{G_{Ae_s}R_s} \tag{10}$$

$$b = \frac{E_i[n]}{G_{AE_i}} \tag{11}$$

$$c = \frac{E_f[n]}{G_{Ae_f}r_L}. \tag{12}$$

The equations of each current mode is switched by comparing *a* and *c* to the critical current *Ic* as shown in Figs. 3 and 4. *a* and *c* are regarded as CCM when they are larger than *Ic*, and then, (6) and (8) are used. On the other hand, *a* and *c* are regarded as DCM when they are smaller than *Ic*, and then, (7) and (9) are

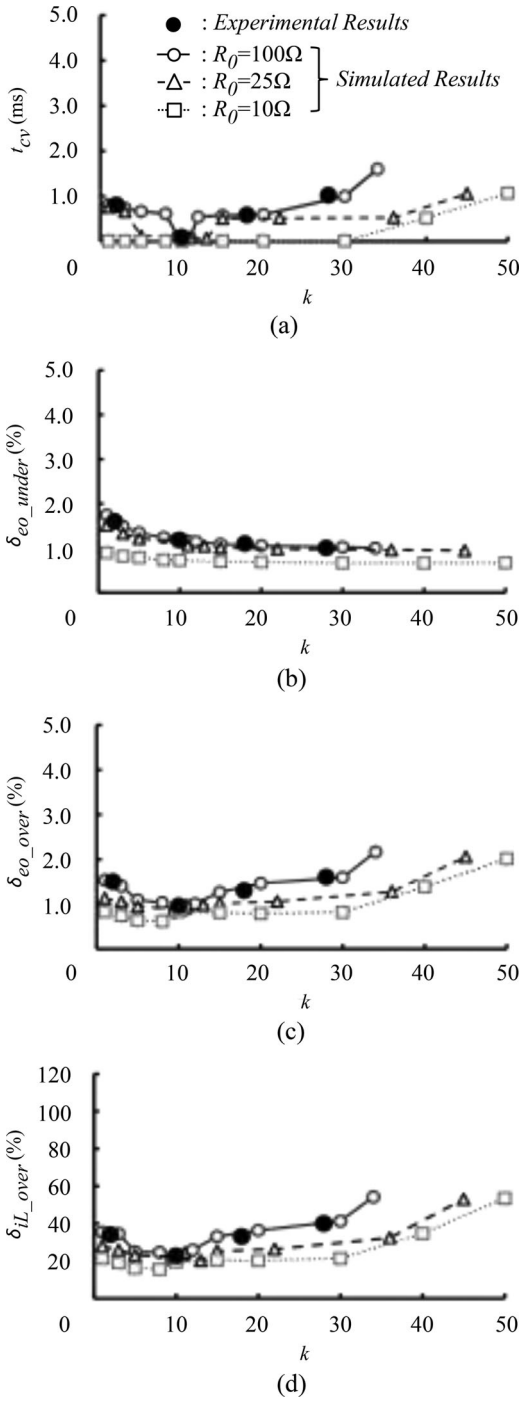

Fig. 8. Transient characteristics by output current sensing. (a) Convergence time for output voltage. (b) Undershoot for output voltage. (c) Overshoot for output voltage. (d) Overshoot for reactor current.

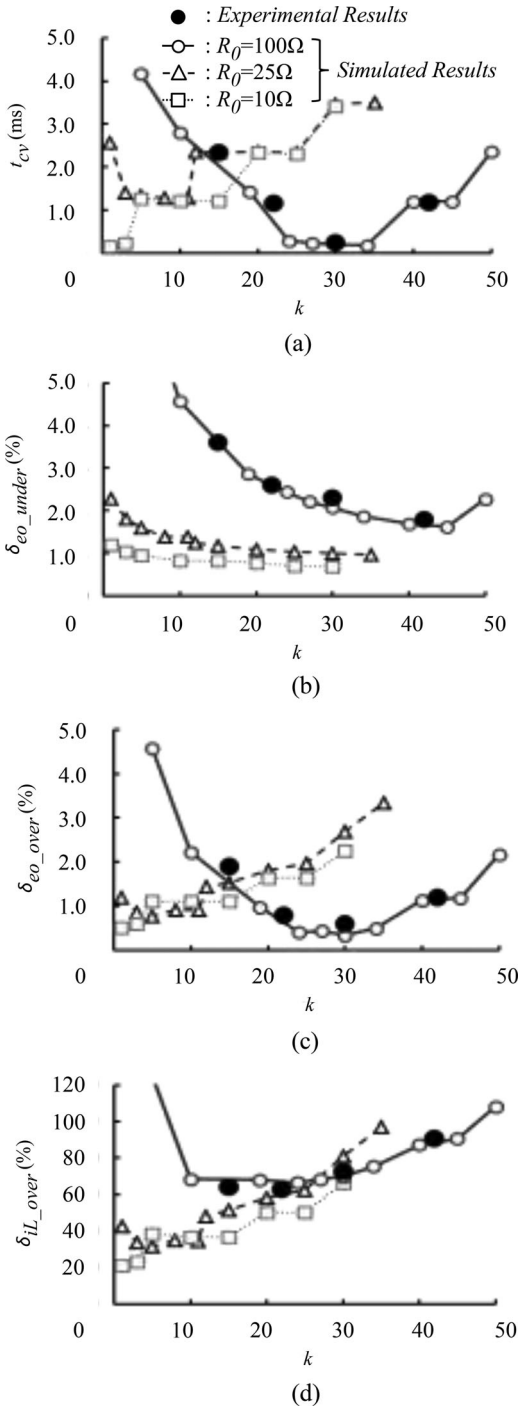

Fig. 9. Transient characteristics by reactor current sensing. (a) Convergence time for output voltage. (b) Undershoot for output voltage. (c) Overshoot for output voltage. (d) Overshoot for reactor current.

used. $T_{on\_mx}[n+1]$ is subtracted as following equation by the subtractor and the bias of PID control is controlled:

$$T_{on}[n+1] = T_{on\_mx}[n+1] - T_{on\_c}[n+1]. \quad (13)$$

$T_{on}[n+1]$ is the digital value corresponding to the on time, and $T_{on\_c}[n+1]$ is the calculation result by the PID control.

Fig. 5 shows the operation characteristics of the proposed method. Fig. 5(a) shows the operation characteristics for bias. The dotted line shows the conventional PID control method, and the solid line shows the proposed method. In the conventional PID control method, the integral control regulates e_o. On the other hand, the proposed method regulates e_o because the bias is calculated for change of I_o by the static

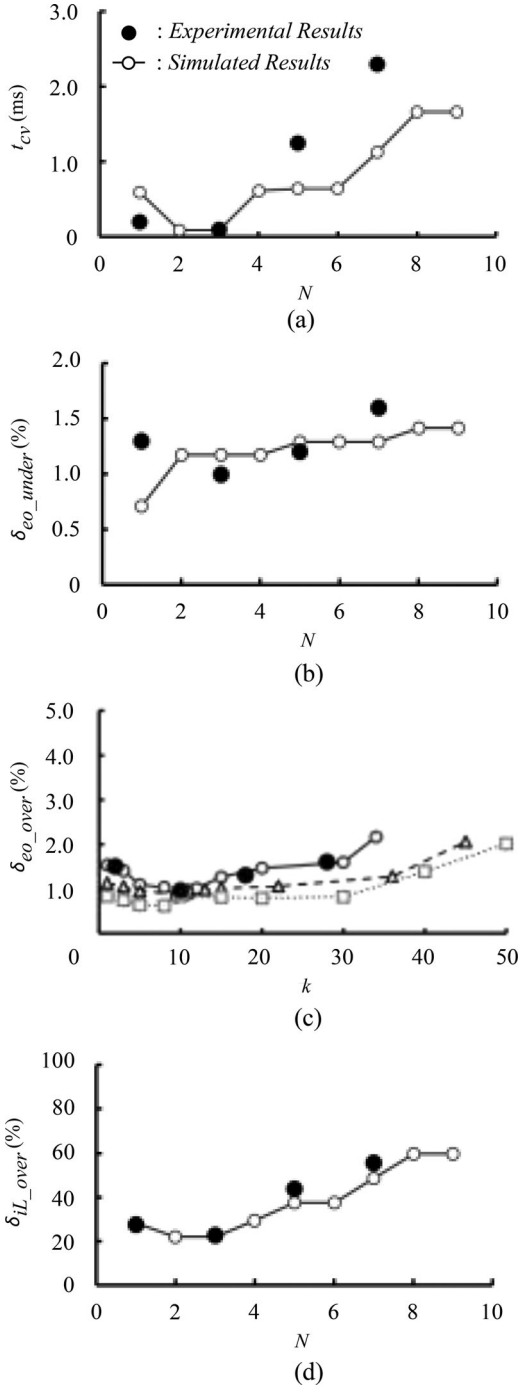

Fig. 10. Influence of reactance moving average by output current sensing. (a) Convergence time for output voltage. (b) Undershoot for output voltage. (c) Overshoot for output voltage. (d) Overshoot for reactor current.

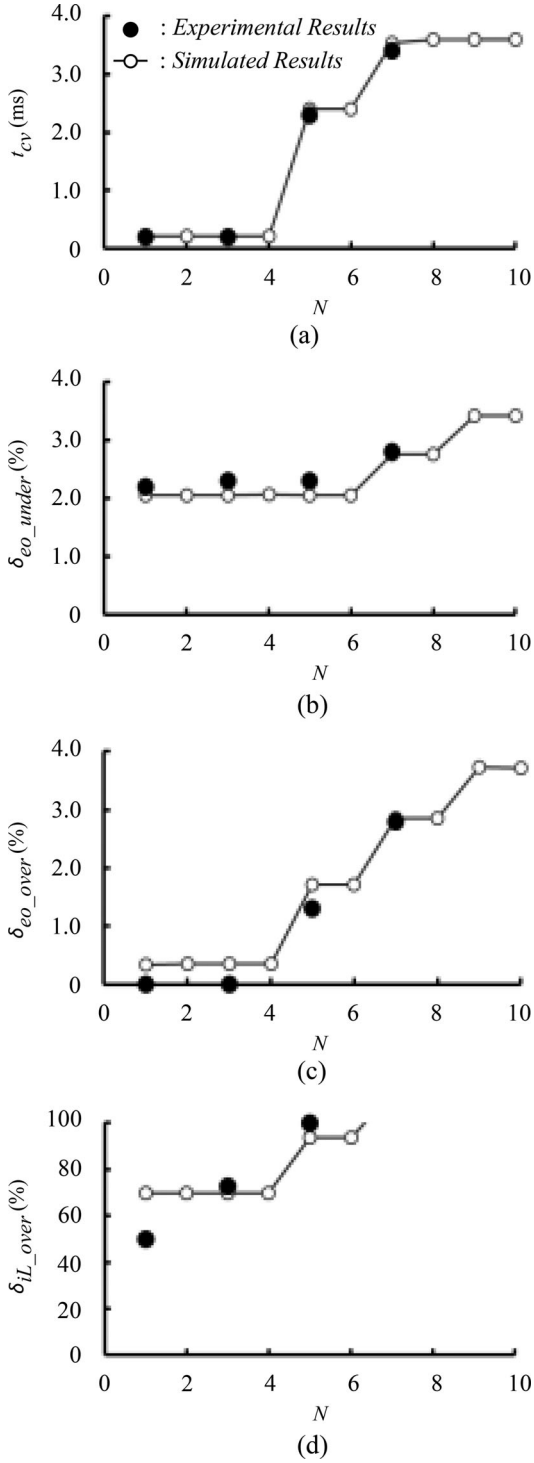

Fig. 11 Influence of reactance moving average by reactor current sensing. (a) Convergence time for output voltage. (b) Undershoot for output voltage. (c) Overshoot for output voltage. (d) Overshoot for reactor current.

model. Therefore, since the proposed method is able to obtain good regulation characteristics without depending on the integral control, the design of integral coefficient can be relatively small.

In the PID controller, the following equation makes $T_{on\_c}[n+1]$:

$$T_{on\_c}[n+1] = K_P\left(e_o[n] - N_{R\_m,n+1}\right) + K_I \sum N_{I,n} + K_D N_{D,n}. \quad (14)$$

In (14), N_R is the constant reference, $\Sigma N_{I,n}$ and N_D are the calculation result of integral control and differential control. K_P is the proportional coefficient, K_I is the integral coefficient, and K_D is the differential coefficient. N_{R_m} is the reference in the proportional control; it is a constant value (N_R) in the steady state. On the other hand, N_{R_m} is modified as shown in the

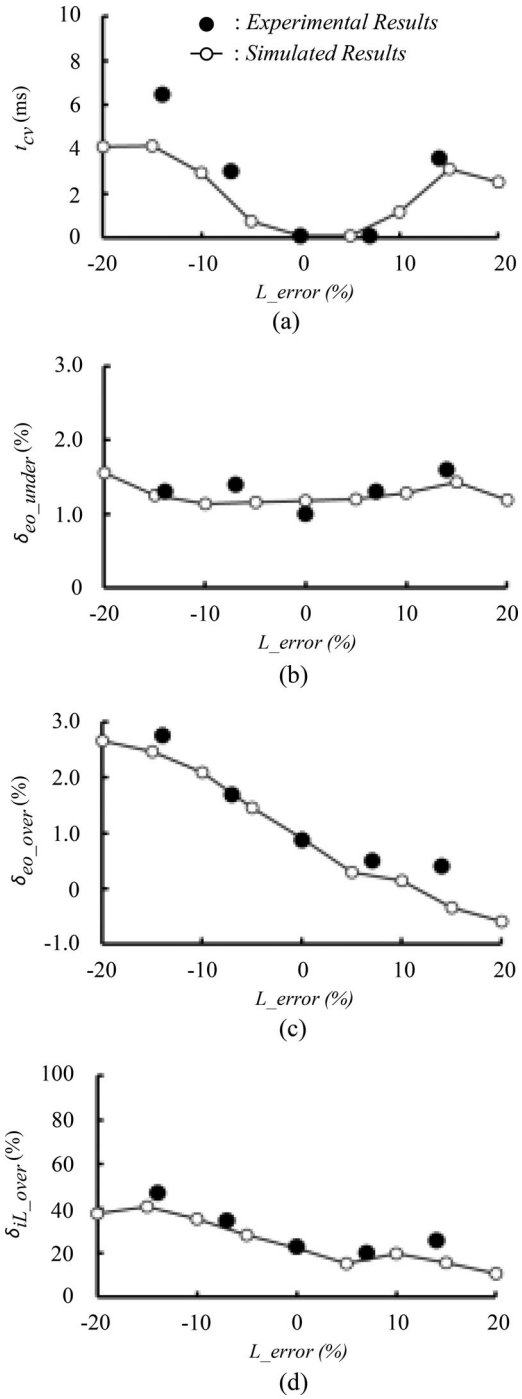

Fig. 12. Influence of reactance L in model by output current sensing. (a) Convergence time for output voltage. (b) Undershoot for output voltage. (c) Overshoot for output voltage. (d) Overshoot for reactor current.

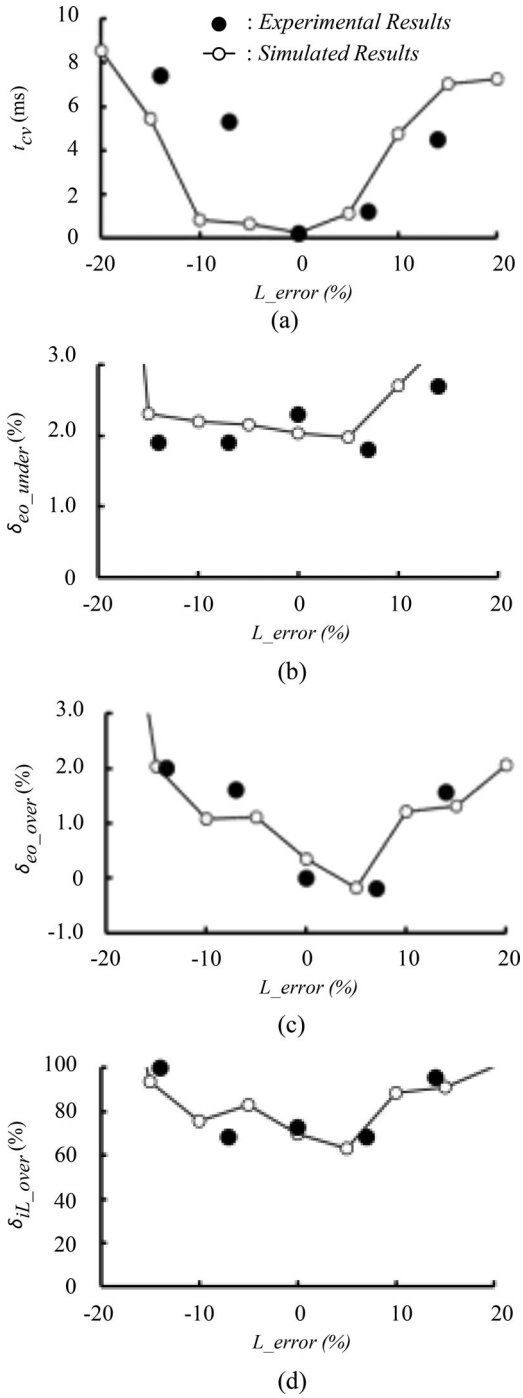

Fig. 13. Influence of reactance L in model by reactor current sensing. (a) Convergence time for output voltage. (b) Undershoot for output voltage. (c) Overshoot for output voltage. (d) Overshoot for reactor current.

following equation only in the transient state:

$$N_{R\_m,n+1} = T_{on\_mx}[n+1] - k\left(e_o[n] - N_R\right). \quad (15)$$

In (15), the control coefficient k determines the amplitude of N_{R_m}. Fig. 5(b) shows the operation characteristics of N_{R_m} based on Figs. 3 and 4. In Figs. 3 and 4, $|\Delta e_o[n]|$ is the absolute value—difference between $e_o[n]$ and $N_{\rm R}$—is divided by N_R and multiplied by 100 to indicate the percentage. N_{R_m} is calculated by (15) when $|\Delta e_o[n]|$ is larger than voltage threshold (VT), and the modification is terminated when the first undershoot $\delta e_o[n]$_under of $e_o[n]$ has reached the maximum value. In this case, a moving average method is applied for $|\Delta e_o[n]|$ in order to avoid the false operation by a noise; it is dependent on a sample number N. The other filter has a relatively long calculation time. The calculation of moving average method is a very simple, and the calculation time is very short. In any other case, N_{R_m} is

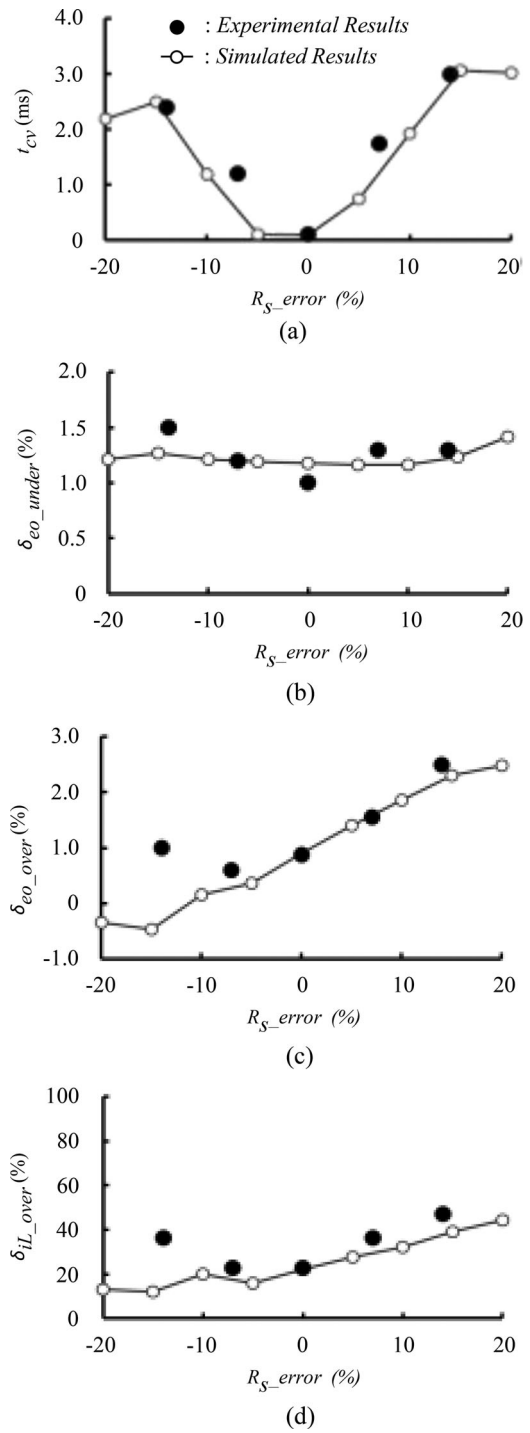

Fig. 14. Influence of sensing resistor R_s in model by output current sensing. (a) Convergence time for output voltage. (b) Undershoot for output voltage. (c) Overshoot for output voltage. (d) Overshoot for reactor current.

N_R. In other words, k changes K_P in the transient state because the following approximate equation is obtained by substituting (15) into (14):

$$T_{on\_c}[n+1] = K_P(1+k)(e_o[n] - N_R) + K_I \sum N_{I,n} + K_D N_{D,n} \quad (16)$$

$$T_{on,n+1} = \left(\frac{T_{on}[n+1]}{N_{T_s}}\right) T_s. \quad (17)$$

III. Performance Characteristics

Therefore, the ripple of e_f is integrated by the low-pass filter in the preamplifier; the averaged reactor current I_L is used in the static model. The cutoff frequency f_c of the low-pass filter is 26 Hz to suppress the ripple of reactor current i_L completely.

Fig. 6 shows the comparison of performance loss against each current-sensing method. The loss of about 1% occurs because R_s is 0.05 Ω in the output current-sensing method. On the other hand, since the *R–C* filter senses i_L in order to decrease the loss. Since R_f of *R–C* filter is 94.6 kΩ, the loss is about 0.048%. Thus, the loss is relatively low about 95% as compared to the output current-sensing method.

Fig. 7 shows the experimental result for regulation characteristics of each control method against the change of I_o. E_i is set to 20 V. The coefficients in (14) are $K_P = 4$ and $K_D = 4$. In case of converting these coefficients to a proportional sensitivity H_P and a differential sensitivity H_D by [19], $H_P = 0.2\ \mathrm{V}^{-1}$ and $H_D = 2\ \mu\mathrm{V/s}$. The good regulation characteristic is easily obtained because the static model operates as the feed forward against the change of I_o. As a result, the proposed method has no steady-state error even when K_I is 0.0008. In this case, an integral sensitivity H_I is equal to $H_I = 4\ \mathrm{s}^{-1} \cdot \mathrm{V}^{-1}$. However, in the conventional PID control method, the regulation range for e_o is impractical in the case of $K_I = 0.0008 (H_I = 4)$. Then, K_I over $0.016 (H_I = 80)$ is necessary to regulate e_o under the same condition of K_P and K_D. Therefore, the proposed method is able to design K_I of 1/20th against the conventional PID control method.

Next, some parameters of model equations through (6) to (9) will be discussed.

Fig. 8 shows the transient characteristics of the output current-sensing method for k in case of taking R_o as a parameter. R_o is the load before the step change. In this case, R_o changes to 10, 25, and 100 Ω as the parameter, and the load R_1 after the step change is set to 5 Ω. The value 5 Ω corresponds to the rated value of dc–dc converter, and the values less than 50 and 100 Ω correspond to CCM and DCM, respectively. In Fig. 8(a)–(d), the filled circle shows the experimental result from $R_o = 100$ W to $R_1 = 5$ W; it is nearly equal to the simulated result. $K_P = K_D = 4$, VT = 0.5% and $N = 3$.

In Fig. 8, the evaluation item is t_{cv}, $\delta e_{o\_\mathrm{under}}$, $\delta e_{o\_\mathrm{over}}$, and $\delta i_{L\_\mathrm{over}}$. t_{cv} is the duration time until e_o is converged within ±1%. $\delta e_{o\_\mathrm{under}}$ and $\delta e_{o\_\mathrm{over}}$ are the undershoot and the overshoot values for e_o. $\delta i_{L\_\mathrm{over}}$ is the overshoot value for i_L. In Fig. 8(a)–(d), each characteristics are improved as k gets larger. Furthermore, the effective range against k becomes narrow as R_o gets larger in Fig. 8(a), (c), and (d); k more than 10 has a negative impact on them in terms of $R_o = 100\ \Omega$. As a result, the proposed method by the output current-sensing method is able to suppress the transient characteristics against various widths of the load for the step change in case of $k = 10$. In case of the transient state, the relational equation for H_P is different from the one in [28], because the reference in *P* control is modify by

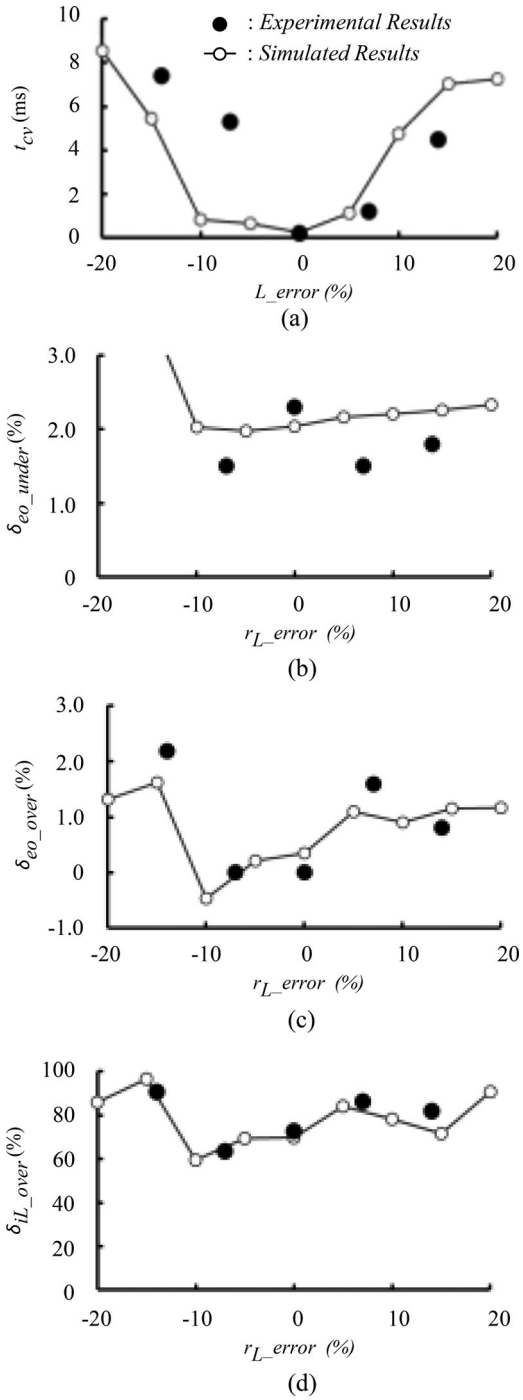

Fig. 15. Influence of ESR r_L of reactor in model by reactor current sensing. (a) Convergence time for output voltage. (b) Undershoot for output voltage. (c) Overshoot for output voltage. (d) Overshoot for reactor current.

(15). The following equation shows the relational equation of H_P for the proposed method in the transient state

$$H_P = \frac{K_P(1+k)A_{e_o}G_{e_o}}{N_{T_s}}. \tag{18}$$

Therefore, H_P is equal to $H_P = 2.2\ \mathrm{V}^{-1}$ in the transient state.

Fig. 9 shows the transient characteristics of the reactor current-sensing method for k in case of taking R_o as a parameter. In this case, R_o changes to 10, 25, and 100 Ω as the parameter. The load after the step change is set to 5 Ω. The ffour filled points are the experimental results from $R_o = 100\ \Omega$ to $R_1 = 5\ \Omega$; it is nearly equal to the simulated result. In Fig. 9(a)–(d), $K_P = K_D = 4$, VT $= 0.5\%$, and $N = 3$. In Fig. 9, the evaluation item is t_{cv}, $\delta e_{o\_\mathrm{under}}$, $\delta e_{o\_\mathrm{over}}$, and $\delta i_{L\_\mathrm{over}}$. In Fig. 9(a)–(d), k which can be most suppressed each characteristics becomes large as R_o get larger. These results are dependent on the integral effect by the low-pass filter for c. Therefore, the optimum values of k against the step changes from 10, 25, and 100 Ω are 1, 8, and 30, respectively. Furthermore, each proportional sensitivity H_P is 0.4, 1.8, and 6.2 V^{-1}, respectively. In the reactor current-sensing method, the optimum value of k is different to the output current-sensing method. The transient response of sensing value of reactor current is slow because the reactor current-sensing method has a low cutoff frequency 26 Hz filter in the preamplifier. In this method, the transient response of $N_{R_m,n+1}$ becomes slow. Therefore, as mentioned earlier, the large value of k is set to increase $N_{R_m,n+1}$ extremely like $k = 30$ in (15). The different values of k are selected to suppress the convergence time t_{cv} perfectly; in general, $k = 20$ is also selected in both methods to suppress all parameters evenly in these figures.

Figs. 10 and 11 show the influence of moving average. Step change of load is from 100 Ω in DCM to 5 Ω in CCM. The tendency of experimental results is similar to that of simulated results. In these figures, it is revealed that $N = 3$ is suitable in both within two methods from the results of transient characteristics.

Figs. 12–15 show the influence of reactance L, ESR r_L of reactor and sensing resistor R_s in the model. Generally, the measurement error of reactance L, ESR r_L of reactor and sensing resistor R_s are within several percents. Therefore, the aforementioned result suggests that both model methods promise to present accurate results. Although t_{cv} becomes relatively large when the error of reactance L in the model exceeds $\pm 5\%$, the other characteristics are kept within $\pm 10\%$ change of L in the model.

In the output current-sensing method, the influence of error R_s in the model is discussed in Fig. 14. Step change of load is from 100 Ω in DCM to 5 Ω in CCM. It is seen that R_s does not affect t_{cv} within $\pm 5\%$ R_s error in the model. The change of characteristics of $\delta e_{o\_\mathrm{under}}$, $\delta e_{o\_\mathrm{over}}$, and $\delta i_{L\_\mathrm{over}}$ are suppressed within $\pm 10\%$ R_s error in the model. As shown in Fig. 15, the tendency of all the parameters is similar to Figs. 12–14. As a result, the experimental results are broadly consistent with simulated results and the proposed method works well within $\pm 5\%$ error in both methods.

Figs. 16 and 17 show the simulated and the experimental transient characteristics from 100 Ω (50 mA) in DCM to 5 Ω (1 A) in CCM by the conventional PID control method. In these figures, Figs. (a) and (b) correspond to the output voltage e_o and reactor current i_L, respectively. In this case, the coefficients in (14) are $K_P = 4$, $K_I = 0.016$, and $K_D = 4$. The output voltage e_o and reactor current i_L are normalized by the desired voltage E_o^* and the rated output current I_o^* in these figures. In

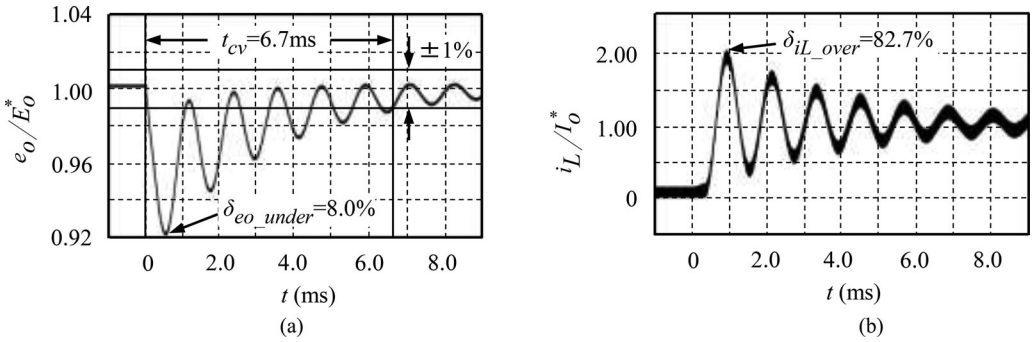

Fig. 16. Simulated results of conventional PID control method. (a) Output voltage. (b) Reactor current.

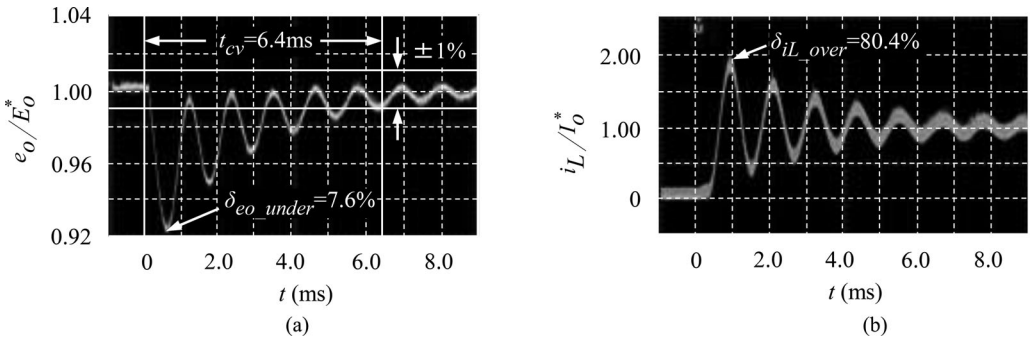

Fig. 17. Experimental results of conventional PID control method. (a) Output voltage. (b) Reactor current.

Fig. 16, t_{cv} is 6.7 ms, $\delta e_{o\_\mathrm{under}}$ is 8.0%, and $\delta i_{L\_\mathrm{over}}$ is 82.7%. In Fig. 17, t_{cv} is 6.4 ms and $\delta e_{o\_\mathrm{under}}$ and $\delta i_{L\_\mathrm{over}}$ are 7.6% and 80.4%, respectively. As a result, the conventional PID control method has limitations in order to improve sufficiently the transient characteristics.

Figs. 18 and 19 show the simulated and the experimental transient characteristics from 100 Ω in DCM to 5 Ω in CCM by the proposed method using the output current-sensing method. Each figure is included for e_o, i_L, N_{Ton_mx}, N_{R_m}, N_{Ton_c}, and T_{on} [n]. Not only e_o and i_L but also N_{Ton_mx}, N_{R_m}, N_{Ton_c}, and $T_{on}[n]$ are normalized by $T_s[n]$. $T_s[n]$ is fixed to 2000 for simple calculation although the number of bits of A–D converter is 11. In this case, K_P is equal to 4, K_I is 0.0008, K_D is 4, VT is 0.5%, and N is 3. These experimental results are obtained under the condition of the filled circle at $k = 10$ in Fig. 8. In Fig. 18, t_{cv} is 0.09 ms, $\delta e_{o\_\mathrm{under}}$ is 1.2%, and $\delta i_{L\_\mathrm{over}}$ is 22.7%. In this case, N_{Ton_mx} is changed based on (6) and (7), and N_{Ton_c} has greatly changed because N_{R_m} is modified when the step change for *R*. In other words, K_P changes from 4 ($H_P = 0.2$) to 44 ($H_P = 2.2$) only when (15) is used. Therefore, a large T_{on} [n] is obtained at the moment the step change for load ocurs, and the on time T_{on} becomes long to cancel the deviation by the step change for *R*. In Fig. 19, t_{cv} is 0.12 ms and $\delta e_{o\_\mathrm{under}}$ and $\delta i_{L\_\mathrm{over}}$ are 1.3% and 21.6%, respectively. Experimental results have also superior transient characteristics because calculation values similar to the simulated results. Compared to the conventional PID control method, t_{cv} is improved about 98% and $\delta e_{o\_\mathrm{under}}$ and $\delta i_{L\_\mathrm{over}}$ are improved relatively about 84% and 73%, respectively. As a result, although the proposed method by output current-sensing method has the performance loss of about 1%, it is able to obtain the superior transient characteristics without changing the control parameter *k*.

Figs. 20 and 21 show the simulated and the experimental transient characteristics from 100 Ω in DCM to 5 Ω in CCM by the proposed method using the reactor current-sensing method. Each figure is included for e_o, i_L, N_{Ton_mx}, N_{R_m}, N_{Ton_c}, and $T_{on}[n]$. The coefficients in (14), VT, and *N* are the same as given earlier. These experimental results are obtained when the filled circle is $k = 30$ in Fig. 9. In Fig. 18, t_{cv} is 0.2 ms, $\delta e_{o\_\mathrm{under}}$ is 2.1%, and $\delta i_{L\_\mathrm{over}}$ is 69.7%. Although N_{Ton_mx} changes based on (8) and (9), it shows gradual changes as compared to the output current-sensing method by the integral effect of the low-pass filter for *c*. Therefore, N_{Ton_c} has to depend on relatively large *k* in N_{R_m} in order to improve the transient characteristics, which is equal to variation K_P from 4 ($H_P = 0.2$) to 124 ($H_P = 6.2$) only when (15) is used. Therefore, T_{on} [n] is calculated to a large value at the moment the step change for load occurs; it controls T_{on} to improve the transient characteristics. In this case, the overshoot of reactor current is reduced to less than 60% when the smoothing capacitor doubles. In Fig. 21, t_{cv} is 0.3 ms and $\delta e_{o\_\mathrm{under}}$ and $\delta i_{L\_\mathrm{over}}$ are 1.6% and 63.6%, respectively. The experimental results are nearly equivalent to the simulated results. Compared to the conventional PID control method, t_{cv} is improved about 96% and $\delta e_{o\_\mathrm{under}}$ and $\delta i_{L\_\mathrm{over}}$ are improved relatively about 76% and 18%.

In the application for the pulse load, from almost no load (50 mA) to the full load (1 A), the convergence time of output

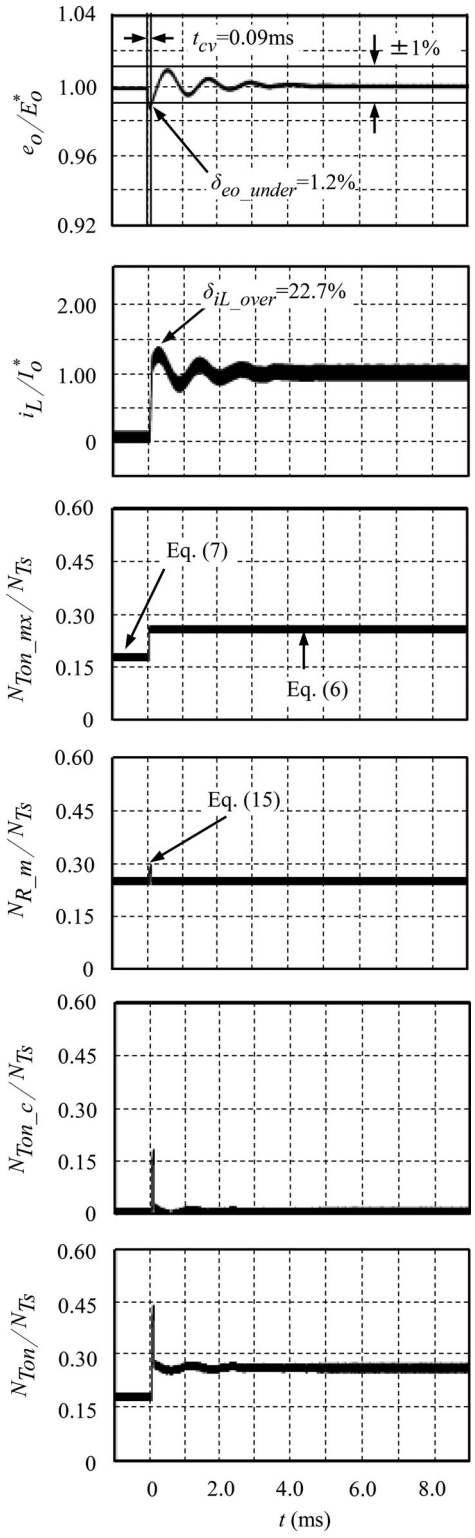

Fig. 18. Simulated results of proposed method by output current sensing.

voltage is 10 ms as shown in Figs. 18–21. On the other hand, in case of the load step from the full load (1 A) to almost no load (50 mA), the convergence time is 80 ms. Therefore, the maximum frequency of pulse load step is about 11 Hz and the minimum pulse widths are 10 and 80 ms, respectively. When the frequency of pulse step exceeds 11 Hz, the output voltage

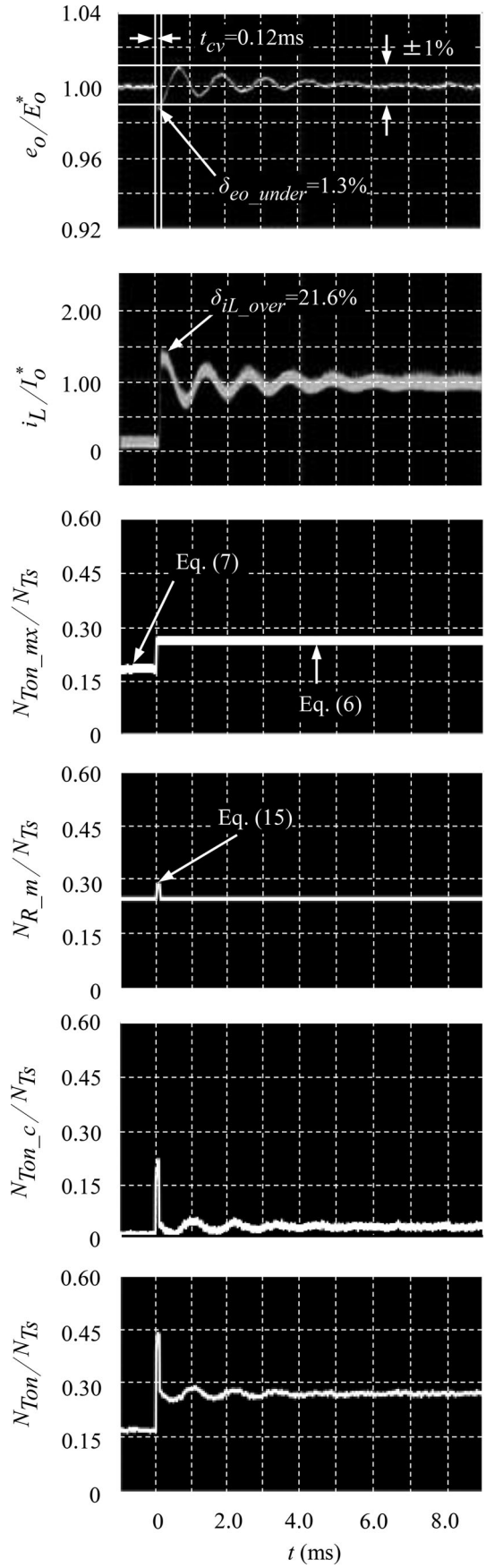

Fig. 19. Experimental results of proposed method by output current sensing.

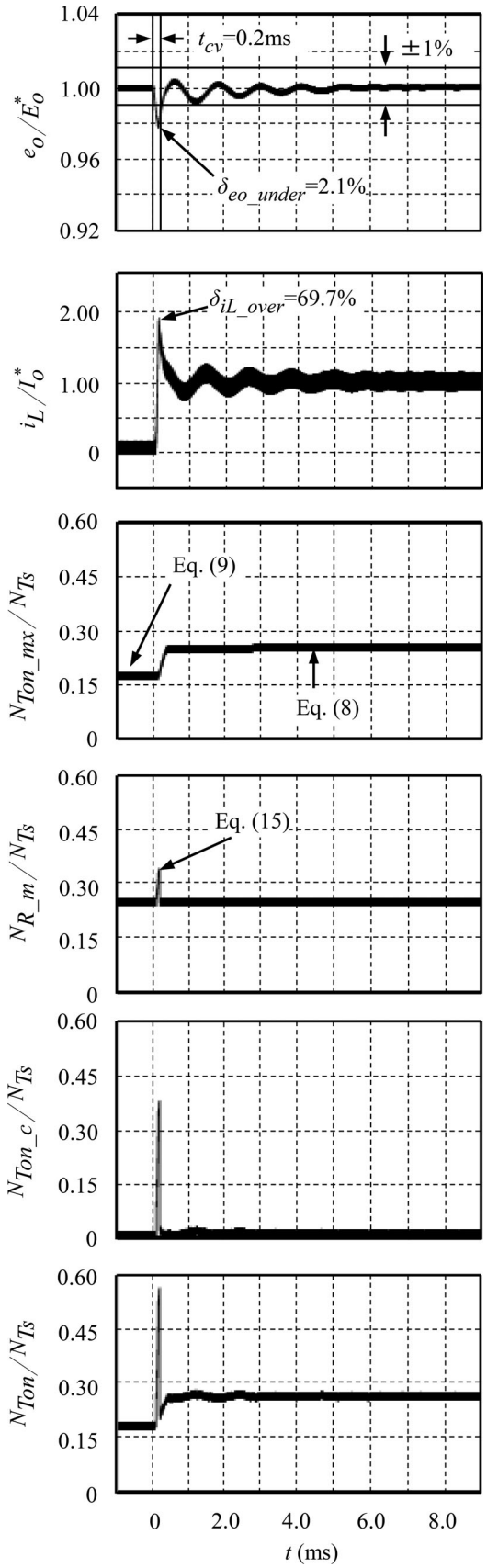

Fig. 20. Simulated results of proposed method by reactor current sensing.

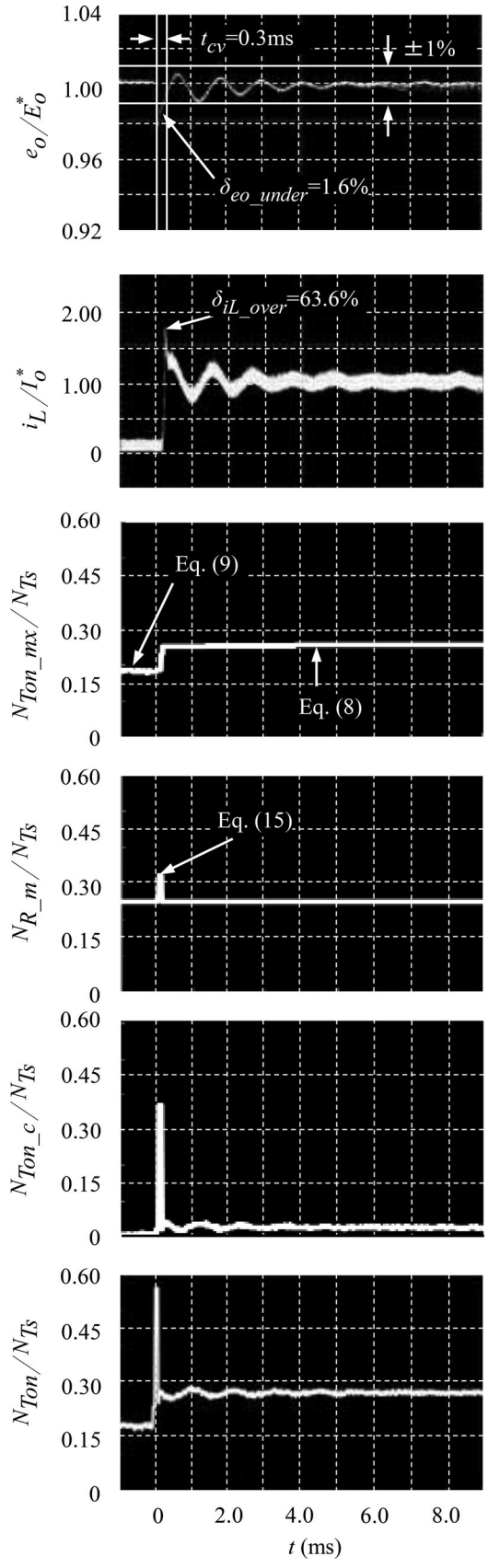

Fig. 21. Experimental results of proposed method by reactor current sensing.

does not converge to the steady state because the next pulse step occurs.

The parameter variations are investigated in Figs. 18–21. Even if the internal resistor r and the output capacitor C vary within 10%, the undershoot of output voltage and overshoot of reactor current are almost the same. The convergence time becomes 10 to 20 times of the designed value because the convergence time is defined when the output voltage converges to 1% of desired output voltage. When the convergence time is defined as the time when the output voltage converges to 2% of the desired output voltage, there is no difference in the convergence time.

We focus on the undershoot of output voltage and the overshoot of reactor current in this paper. The presented method achieves the small undershoot of output voltage and the suppressed overshoot of reactor current compared with not only the PID control method but also the adaptive control method in [29]–[32]. However, the underdamped oscillation still exists.

To suppress the underdamped oscillation, the proposed method has the possibility to combine the adaptive control method published in [30]–[32].

As a result, in the proposed method by reactor current-sensing method, although the integral effect of the low-pass filter has an impact on the transient characteristics, the performance loss is very small.

Therefore, the output current-sensing method is effective in case high-transient-response performance is required. On the other hand, it is better to use the reactor current-sensing method when the efficiency is important.

IV. Conclusion

The proposed method is able to improve transient characteristics because it modifies the reference of conventional PID control method against the change of output voltage. This paper discusses two current-sensing methods for the proposed method. In the output current-sensing method, it is confirmed that the undershoot of output voltage and the overshoot of reactor current are improved by about 84% and 73% as compared to the conventional PID control method against the step change from DCM to CCM. In the reactor current-sensing method, the undershoot of output voltage and the overshoot of reactor current are improved by about 76% and 18% without sacrificing the performance loss. As a result, the output current-sensing method is effective in case that high-transient-response performance is required. On the other hand, it is better to use the reactor current-sensing method when the efficiency is important. Although the proposed method improved the undershoot of output voltage and the overshoot of reactor current compared with not only the PID control method but also the adaptive control method, the underdamped oscillation still exists. The proposed method has the possibility to combine the adaptive control method for the suppression of the underdamped oscillation. We will present a new superior model control combined with the adaptive control to regulate the output voltage under the all-around load and input voltage conditions in the near future.

References

[1] K. De Cuyper, M. Osee, F. Robert, and P. Mathys, "A digital plat form for real-time simulation of power converters with high switching," in *Proc. IEEE Power Electron. Appl.*, pp. 1–10, Sep. 2011.

[2] G. Feng, E. Meyer, and Y. Liu, "A new digital control algorithm to achieve optimal dynamic performance in dc-to-dc converters," *IEEE Trans. Power Electron.*, vol. 22, no. 4, pp. 1489–1498, Jul. 2007.

[3] S. Saggini, M. Ghioni, and A. Geraci, "An innovative digital control architecture for low-voltage, high-current dc–dc converters with tight voltage regulation," *IEEE Trans. Power Electron.*, vol. 19, no. 1, pp. 210–218, Jan. 2004.

[4] S. Chattopadhyay and S. Das, "A digital current-mode control technique for dc–dc converters," *IEEE Trans. Power Electron.*, vol. 21, no. 6, pp. 1718–1726, Nov. 2006.

[5] L. Corradini, E. Orietti, P. Mattavelli, and S. Saggini, "Digital hysteretic voltage-mode control for dc–dc converters based on asynchronous sampling," *IEEE Trans. Power Electron.*, vol. 24, no. 1, pp. 201–211, Jan. 2009.

[6] D. Segaran, D. G. Holmes, and B. P. McGrath, "Enhanced load step response for a bidirectional dc–dc converter," *IEEE Trans. Power Electron.*, vol. 28, no. 1, pp. 371–379, Jan., 2013.

[7] P. Shangzhi and P. K. Jain, "A low-complexity dual-voltage-loop digital control architecture with dynamically varying voltage and current references," *IEEE Trans. Power Electron.*, vol. 29, no. 4, pp. 2049–2060, Apr. 2014.

[8] M. Castilla, L. G. de Vicuna, J. M. Guerrero, J. Matas, and J. Miret, "Disigning vrm hysteretic controllers for optimal transient response," *IEEE Trans. Power Electron.*, vol. 22, no. 4, pp. 1726–1738, Jun. 2007.

[9] K. Yao, Y. Ren, and F. C. Lee, "Critical bandwidth for the load transient response of voltage regulator madules," *IEEE Trans. Power Electron.*, vol. 19, no. 6, pp. 1454–1461, Nov. 2004.

[10] G. Zhou and J. Xu, "Digital average current controlled switching dc–dc converters with single-edge modulation," *IEEE Trans. Power Electron.*, vol. 25, no. 3, pp. 786–793, Mar. 2010.

[11] E. Meyer and L. Yan-Fei, "Digital charge balance controller with an auxiliary circuit for improved unloading transient performance of buck converters," *IEEE Trans. Power Electron.*, vol. 28, no. 1, pp. 357–370, Jan. 2013.

[12] H. Zhiyuan, L. Yan-Fei, T. Yeap, and G. Lusheng, "A communication protocol with data compression for isolated digital power supplies," *IEEE Trans. Power Electron.*, vol. 29, no. 4, pp. 2109–2123, Apr. 2014.

[13] S. Pan and P. K. Jain, "Novel digital control architecture with non-linear control algorithms exhibiting very fast transient response," in *Proc. IEEE Appl. Power Electron. Conf. Expo.*, 2009, pp. 1497–1503.

[14] A. Babazadeh and D. Maksimovic, "Hybrid digital adaptive control for fast transient response in synchronous buck dc–dc converters," *IEEE Trans. Power Electron.*, vol. 24, no. 11, pp. 2625–2638, Nov. 2009.

[15] F. Kurokawa, K. Tanaka, H. Eto, and H. Matsuo, "Dynamic characteristics of switching dc–dc power converter with static model reference," in *Proc. IEEE Int. Telecommun. Energy Conf.*, Sep. 2005, pp. 421–426.

[16] H. Matsuo, F. Kurokawa, and H. Eto, "Novel digital controller with static model reference for switching dc–dc power," *IEEE Trans. Power Electron.*, vol. E88-B, no. 11, pp. 4346–4352, Nov. 2005.

[17] H. Matsuo, F. Kurokawa, H. Eto, N. Suzuki, and Y. Makino, "Novel digital controller with statics model reference for switching dc–dc power converters," in *Proc. IEEJ Int. Power Electron. Conf.*, vol. 3, pp. 1997–2001, Mar. 2000.

[18] F. Kurokawa and S. Sukita, "A new model control dc–dc converter to improve dynamic characteristics," in *Proc. IEEE Power Electron. Drive Syst.*, pp. 763–767, Nov. 2007.

[19] F. Kurokawa, J. Sakemi, A. Yamanishi, and H. Osuga, "A new STS model DC–DC converter," in *Proc. IEEE Energy Convers. Congr. Expo.*, Sep. 2011, pp. 680–684.

[20] F. Kurokawa, J. Sakemi, A. Yamanishi, and H. Osuga, "A new auto-bias method for digital control dc–dc converter," in *Proc. IEEE Int. Conf. Electr. Mach. Syst.*, Aug. 2011, pp. 1–5.

[21] F. Kurokawa, J. Sakemi, A. Yamanishi, and H. Osuga, "A new quick transient response digital control dc–dc converter with smart bias function," in *Proc. IEEE Int. Telecommun. Energy Conf.*, Oct. 2011, pp. 1–7.

[22] Z. Lukic, Z. Zhao, S. M. Ahsanuzzaman, and A. Prodic, "Self-tuning digital current estimator for low-power switching converters," in *Proc. IEEE Appl Power Electron. Conf. Expo.*, Feb. 2008, pp. 529–534.

[23] Y. F. Li, M. F. Tsai, C. S. Tseng, and Y. F. Chiang, "Model reference adaptive control design for the buck-boost converter," in *Proc. Annu. Conf. IEEE Ind. Electron. Soc.*, Oct. 2012, pp. 543–548.

[24] P. Karamanakos, T. Geyer, and S. Manias, "Direct model predictive current control strategy of DC–DC boost converters," *IEEE J. Emerging Sel. Topics Power Electron.*, vol. 1, no. 4, pp. 337–346, Dec. 2013.
[25] C. G. R, S. W. I, and P. J. O, "Takagi-Sugeno Fuzzy model and control of a boost converter using type-i internal model control," in *Proc. Annu. Conf. IEEE Ind. Electron. Soc.*, Nov. 2013, pp. 3794–3799.
[26] P. Liu, F. C. Lee, and Q. Li, "Modeling and autotuning of AVP control with inductor DCR current sensing," in *Proc. IEEE Appl. Power Electron. Conf. Expo.*, Mar. 2014, pp. 1066–1072.
[27] H. Matsuo and K. Harada, "Characteristics of dc–dc converter in the discontinuous mode of the reactor current," *Trans. IEICE Japan*, vol. J93-C, no. 6, pp. 123–129, Jun. 1973.
[28] Y. Nakao, Y. Mimura, F. Kurokawa, and H. Matsuo, "A consideration of digital control circuit for dc–dc converter," *Inst. Electron., Inf. Commun. Eng., Japan, Tech. Report EE97*, Feb. 1998, pp. 13–20.
[29] F. Kurokawa, J. Sakemi, A. Yamanishi, and H. Osuga, "A new sts model dc–dc converter," in *Proc. IEEE Energy Convers. Congr. Expo.*, pp. 680–684, Oct. 2011.
[30] F. Kurokawa and S. Higuchi, "A novel digital variable integral gain control for dc–dc converter," in *Proc. IEEE Electr. Mach. Syst.*, Oct. 2012, pp. 1–5.
[31] F. Kurokawa, T. Ishibashi, J. Sakemi, and T, Babasaki, "An auto-tuning digital control for buck-boost dc–dc converter," in *Proc. IEEE Electr. Telecommun. Energy Conf.*, pp. 1–5, Jun. 2010.
[32] A. Costabeber, P. Mattavelli, S. Saggini, and A. Bianco, "Digital autotuning of dc–dc converters based on model reference impulse response," in *Proc. IEEE Appl. Power Electron. Conf. Expo.*, Feb. 2010, pp. 1287–1294.

Fujio Kurokawa (F'11) was born in Yamaguchi, Japan, in 1952. He received the B.S. degree in electronic engineering from the Fukuoka Institute of Technology, Fukuoka, Japan, in 1976, and the Dr. Eng. degree from Osaka Prefecture University, Sakai, Japan, in 1988.

Since 1984, he has been with Nagasaki University, Nagasaki, Japan, where he is currently a Professor and Vice-Dean of Graduate School of Engineering. His current research interests include digital power, switching power supply for telecommunications, solar power supply, power plant control, and ion engine control for satellite.

Dr. Kurokawa is a Fellow of the Illuminating Engineering Institute of Japan, and also a Senior Member of the Institute of Electronics, Information and Communication Engineers of Japan, and the Institute of Electrical Engineers of Japan.

Akihiro Yamanishi received the B.S. degree in electrical and electronic engineering in 2011 from Nagasaki University, Nagasaki, Japan, where he is currently working toward the M.S. degree in the Graduate School of Engineering.

Shota Hirotaki (M'13) was born in Saga Prefecture, Japan, in 1990. He received the B.S. degree in electrical and electronic engineering from Nagasaki University, Nagasaki, Japan, in 2013.

He is currently a Student of the Graduate School of Engineering, Nagasaki University. His current research interests include switching power converters and their digital control.